Single Scanner BLS System for Forest Plots Mapping

Jie Shao, Wuming Zhang, Nicolas Mellado, Shuangna Jin, Lei Luo, Shangshu Cai,
Lingbo Yang, and Guangjian Yan

Abstract—Three-dimensional (3D) structural information collected from sample plots is significant for forest inventories. Terrestrial laser scanning (TLS) has been demonstrated to be an effective instrument in data acquisition of forest plots, but the application of TLS is time consuming and laborious due to the need for scan preparation and its lack of mobility. In contrast, mobile laser scanning (MLS) is being increasingly utilized in the mapping of various environments due to its mobility. However, the geometrical peculiarity of forests (e.g., occlusion, similarity between tree shapes) poses problems for existing mapping methods. In this paper, a backpack-based single scanner MLS system, i.e., backpack laser scanning (BLS), is designed for mobile mapping of forest. Thus, to achieve accurate feature matching, this paper proposes to combine the line and point features for scanner positioning, in which the line feature is derived from trunk skeletons. In addition, an optimization framework based on two incremental maps is proposed for correcting positional drift. Finally, this paper evaluates the effectiveness and the mapping accuracy of the proposed method under forest canopy conditions. The experimental results indicate that the proposed method achieves accurate forest mapping using the BLS system; meanwhile, compared with the previous methods, the proposed method effectively utilizes the geometric characteristics of the tree stems and reaches a lower mapping error, in which the mean errors for the horizontal/vertical direction in plots are less than 2 cm, and the standard deviations are at the millimeter level.

Index Terms—Forest plots, mobile mapping, point cloud, single scanner BLS, SLAM.

I. INTRODUCTION

PRECISE structural information collected from field measurements is necessary for forest inventories, decision making on forest resources, and ecological studies. Most of the field measurements in a forest are based on field sample plots, and these sample plots are typically representative of the entire area of interest [1]. Generally, it is expensive to measure sample plots utilizing conventional and simple measurement tools. With the development of remotely sensed data, a frequently used method of the forest measurements is known as light detection and ranging (LiDAR), and a common LiDAR method uses laser scanners [2], [3]. The precondition of LiDAR-based method is mapping of the surrounding environment [4]. In this context, LiDAR-based mapping has become an active research topic for forest inventories.

Terrestrial laser scanning (TLS), commonly known as ground-based LiDAR, has shown promise in highly accurate forest mapping [5], [6]. TLS instruments use either a pulsed or continuous frequency modulated laser that measures the distance to an intercepting surface and allows for the precise location of the surface to be determined [7]. Currently, common TLS instruments can fire millions of laser pulses per scan, which creates a highly detailed 3D point cloud representation of the scanning domain. However, the occlusion effect limits the use of the instrument in forest environments [8]. To tackle the occlusion effect, multiple TLS scans are typically utilized to scan forest plots instead of one single scan in the center of the plot [9]. For multiple scans, pre-scan preparations are generally required, e.g., placing targets [10], which reduces the cost effectiveness of the technology. As a result, the largest problem with TLS is that it is often a cumbersome and time-consuming task, increasingly hindered by increasing size of the sample plot to be mapped.

Laser scanners have recently been mounted on moving platforms to build mobile laser scanning (MLS) systems and are being studied for forest mapping. Compared to TLS, the main advantage of MLS is the immensely rapid data collection in complex forest environments. Thus, it has great opportunities for increasing the cost effectiveness of TLS instruments [11], [12]. The greatest challenge for MLS is positional accuracy which is closely connected with the accuracy of mapping.

Due to the ability of the global navigation satellite system (GNSS) to position the sensor and the ability of the inertial measurement unit (IMU) to produce the attitude information, the GNSS-IMU system is usually used to derive the trajectory

information of MLS for various mapping tasks [13], [14], [15]. The positioning techniques work correctly in clear sky conditions, but the task becomes increasingly difficult when satellite visibility decreases or multipath effects increase [16]. In forest environments, satellite availability largely depends on the amount of coverage by the canopy, and the dense canopy absorbs, reflects or completely blocks the GNSS radio frequency signal, causing either a poor signal or signal loss. Even with a high precision GNSS-IMU system, the positioning error can grow to several tens of centimeters and even to meters due to trajectory drift and will greatly limit the mapping accuracy in dense forest environments [17]. In such cases, the scanner MLS needs to be repositioned during the mapping step, which leads to the so-called simultaneous localization and mapping (SLAM) problem [18].

SLAM is the process of mapping an unknown environment and locating the mobile platform simultaneously, which has now been widely used to provide positioning information in various environments [19]. In the initial stage of the SLAM technique, a common sensor is a camera, and currently, many excellent methods have been proposed for positioning and mapping based on the camera, e.g., MonoSLAM (MonoSLAM: Real-Time Single Camera SLAM) [20], LSD-SLAM (Large-Scale Direct Monocular SLAM) [21], SVO (SVO: Fast Semi-Direct Monocular Visual Odometry) [22], and ORB-SLAM (ORB-SLAM: A Versatile and Accurate Monocular SLAM System) [23]. However, these methods require a strong matching of landmarks and are generally limited by depth precision. By contrast, LiDAR typically has superior depth perception and the capacity of dense mapping, both in 2D and 3D. Similarly, some LiDAR-based SLAM algorithms have also been developed for positioning and mapping in various environments without reference coordinates, especially the graph-based SLAM approach, such as LOAM (LOAM: Lidar Odometry and Mapping in Real-time) [24] and Cartographer [25]. In the literature, the features, including the point, line, and plane of both the camera-based SLAM technique and the LiDAR-based SLAM technique are usually used to estimate the position and attitude of the sensors. In the feature-based SLAM methods, the position and attitude solution is continuing to mature, but the feature selection limits the effectiveness of the methods in various environments. For MLS data, the feature-based SLAM methods can acquire satisfactory solutions due to rich and clear geometrical features in indoor and urban scenes [26]. However, the features are not stable or continuous in forest environments. In addition, objects in the forests are remarkably similar, which easily causes inaccurate corresponding pairs and registration results. For example, the LOAM method utilizes the line and plane features to achieve SLAM-based mapping and generally needs an initial transformation for feature matching, of which the features are extracted from the objects surface. However, during the nonlinear optimization process the selected features easily fall into local minima when matching is implemented with an inaccurate initial transformation in forest scenes. Therefore, the feature selection poses challenges to the feature-based SLAM methods in accurate mapping of forest scenes.

In practice, many feature-based studies in scan matching have been presented for forest environments, of which manually selected features [27], artificial targets [28], [29] or geometrical features (or "marker-free") [30], [31] are commonly adopted to calculate the position and attitude of scanners. However, these studies mainly serve for coregistration of several dense point clouds, e.g., TLS-TLS data. The process that selects features manually is labor intensive and time-consuming [32] and surely would not be practical for thousands of MLS point clouds; the artificial targets could provide landmarks for localization of the sensor, but they are difficult to extract from the sparse MLS point clouds due to the size of the targets and the effects of occlusion. In addition, the common marker-free-based methods focus on coarse alignment of point clouds and need a fine registration step in postprocessing. The iterative closest point (ICP) method [33] is now the standard approach for fine registration. It starts by searching the corresponding pairs between point clouds, and then minimizes the distance between those pairs. Consequently, the method generally requires sufficient overlap of point clouds for obtaining accurate correspondences. However, the sparsity of MLS data and the lack of points overlap easily leads to inaccurate pairs and affects registration results. Therefore, this method is ill-suited to forest scenes.

MLS-based mapping has increasingly gained attention in various environments. However, the complex structure and irregular shape of the natural elements in the forest brings challenges to the existing mapping methods using MLS [34]. Therefore, we integrate a single scanner BLS system without the GNSS-IMU technique and propose a novel mapping method specific to forest environments in this paper. For accurate positioning, we extract trunk skeletons that represent the tree center lines for motion estimation of BLS, which prevents inaccurate corresponding pairs and allows scan matching with low overlap. In addition, a new optimization framework based on incremental trunk skeletons points and BLS point clouds is used for global optimization and prevents accumulative errors. Following the introduction section, the overview and key steps of the proposed method is elaborated in Section II. Section III introduces the performance of the proposed method on field measurements. Finally, discussions and conclusions are presented.

II. METHODS

A. Outline of the method

In this paper, we focus our attention on forest plots mapping using a single scanner. First, a single scanner BLS system is used for acquisition of raw point clouds. Then, a SLAM-based method is executed for forest plots mapping, which consists of four key components: feature extraction, feature matching, motion estimation, and global optimization. Specifically, we propose the combination of the semantic line features and point features for motion estimation, in which the lines are derived from trunk skeletons that are natural geometric elements of trees, and the point features are extracted from the BLS point cloud evenly. Finally, accumulative BLS point clouds and the

trunk skeleton map are used to provide global constraints and optimize the pose of each BLS point cloud. The proposed processing flowchart is shown in Fig. 1.
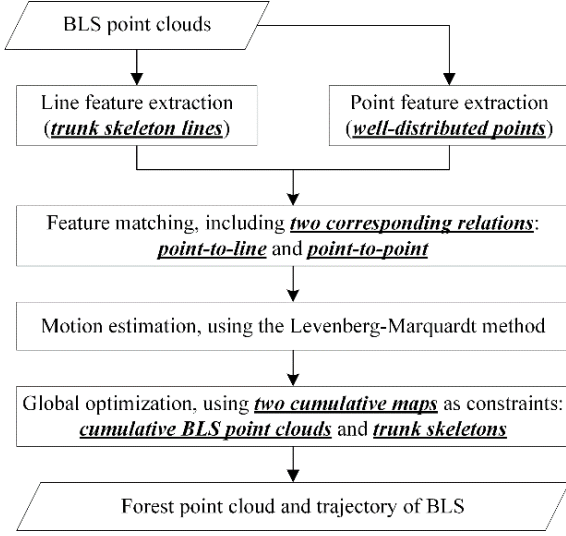

Fig. 1. Flowchart of SLAM-based forest mapping.

B. Feature extraction

In the feature-based SLAM method, feature extraction is the precondition of localization and mapping. To achieve accurate matching, we propose to combine the line and point features to estimate the motion of the scanner in this paper, of which the line features are mainly used to optimize the matching error in the horizontal direction and the point features are used to ensure the vertical accuracy.

1) Line features

For BLS point clouds captured from different positions, accurate corresponding pairs between the two frames are difficult to extract directly due to the sparsity of data and the complexity of natural elements. In the forest, tree trunks are remarkable and stable [35]. Although the surface of the tree trunks rarely has significant geometric features, the tree trunk skeletons that represent the tree center lines can provide stable and robust constraints for motion estimation of the scanner, especially in the horizontal direction. Therefore, we study a hierarchical clustering method to extract the tree trunk skeletons from each frame of the BLS point clouds.

According to the characteristics of the BLS point cloud used, the raw point cloud is first divided into multiple subsets of point clouds based on the angular resolution in the vertical direction. For each subset, distance-based region growing is used to segment various objects, and then the circle fit based on the least square method is used to detect tree trunk points. Finally, the center points of the detected circles are regarded as trunk skeleton nodes, and the nodes that are continuously distributed in the vertical direction are considered to be derived from a trunk skeleton in which the connected line between two neighbor nodes is regarded as a line feature (Fig. 2).
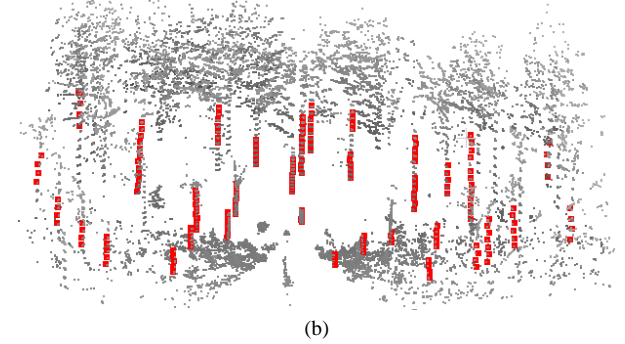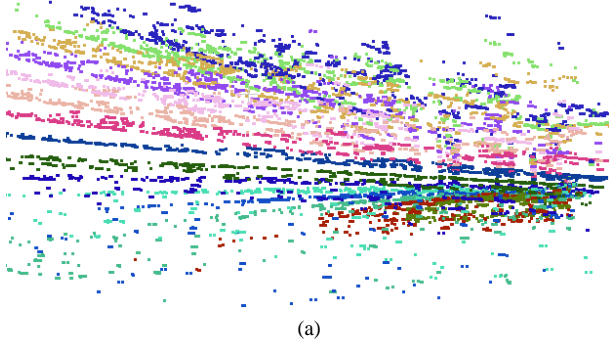

Fig. 2. Line features extraction. (a) Layered processing. Different colors represent subsets of different layers. (b) Extracting tree trunk skeleton nodes (red points), skeleton lines can be generated by connecting the neighboring nodes.

2) Point features

The trunk skeletons contribute to reducing horizontal error of mapping results, but due to the approximate parallel relationship among trunk skeletons, the line features have difficulty providing constraints for feature matching in the vertical direction. Therefore, we use well-distributed points to provide an overall constraint for the SLAM process. In this paper, the *difference of Gaussian* (DoG) method is used to extract point features.

DoG is usually used for feature enhancement and extraction in digital imaging processing. Major advantages of DoG features are their invariance to scaling, rotation and translation [36]. By contrast, we directly extract features based on point range. The principle of DoG-based 3D point feature extraction is subtracting one blurred point cloud level from another blurred point cloud level. The blurred levels are obtained by convolving the point cloud with Gaussian kernels having different standard deviations.

$$\mathcal{F}_i(x,y,z) = G_i(x,y,z;\sigma_1) - G_i(x,y,z;\sigma_2) \tag{1}$$

where $\mathcal{F}_i$ is the difference between the Gaussians of a point (x,y,z) and G is the Gaussian kernel in 1D,

$$G(x,y,z;\sigma) = \frac{1}{\sqrt{2\pi}\sigma} e^{-\frac{(|(x,y,z)|-\mu)^2}{2\sigma^2}} \tag{2}$$

where the σ represents the *width* of the Gaussian kernel. In statistics, σ is the standard deviation and σ^2 is the variance. Finally, we detect points with local minima or maxima $\mathcal{F}$ value as the point feature.

In this paper, 180 feature points were extracted from each frame of the BLS point cloud (see Fig. 3). Let $\mathcal{R}_n^L$ be the set of point features in the time of sweep *n*.
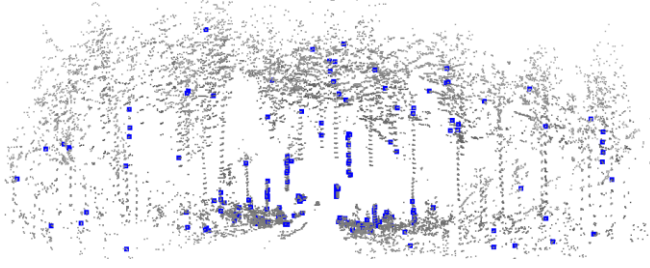
Fig. 3. Point features extraction. Grey points are raw BLS points and blue points represent the extracted real feature points.

C. Feature matching

The acquisition of BLS data is rapid and continuous. Therefore, to find corresponding feature pairs for motion estimation, the Euclidean nearest neighbor search is adopted for feature matching, and the distance between the matched features is regarded as the matching constraint.

For a tree stem, the corresponding trunk skeletons that derived from the BLS point cloud and its reference are similar, but they are not exactly the same because of the sparsity of the BLS data. By contrast, the trunk skeleton nodes maintain uniform distribution with the corresponding trunk skeleton in its reference, so the point-to-line (trunk skeleton node to trunk skeleton line) distance could establish a more accurate

relationship between the BLS point clouds. If a skeleton node has two nearest skeleton points in the reference data which are within a certain neighborhood of the node, then we set the skeleton node as a keypoint and regard the line that is composed by the two nearest skeleton points as a corresponding feature for motion estimation. The distance d_l between the point and line can be computed by

$$d_l = \frac{\left|\left(X_{(t+1,l)} - X_{(t,a)}\right) \times \left(X_{(t+1,l)} - X_{(t,b)}\right)\right|}{\left|X_{(t,a)} - X_{(t,b)}\right|} \tag{3}$$

where $X_{(t+1,l)}$ is a trunk skeleton node at the time of sweep, $t + 1$, and $X_{(t,a)}$ and $X_{(t,b)}$ are the two nearest skeleton points of $X_{(t+1,l)}$ at the time of sweep, t.

In addition, due to fast convergence speed, the planar patch is found to be the correspondence of the point feature. If a point has three nearest points in reference that are within a certain neighborhood and not on the same line, then a planar patch consisting of the three points is regarded as a correspondence of the point feature, and the point will be used as a keypoint for motion estimation. The distance, d_p, between the point and the plane can be computed by

$$d_p = \frac{\left|\overrightarrow{X_{(t+1,p)}X_{(t,a)}} \cdot \vec{n}\right|}{|\vec{n}|} = \frac{\left|\left(X_{(t+1,p)} - X_{(t,a)}\right) \cdot \left(\left(X_{(t+1,p)} - X_{(t,b)}\right) \times \left(X_{(t+1,p)} - X_{(t,c)}\right)\right)\right|}{\left|\left(X_{(t+1,p)} - X_{(t,b)}\right) \times \left(X_{(t+1,p)} - X_{(t,c)}\right)\right|} \tag{4}$$

where $X_{(t+1,p)}$ is a feature point at the time of sweep, $t + 1$, and its corresponding plane at the time of sweep, t, is set to $\{X_{(t,a)}, X_{(t,b)}, X_{(t,c)}\}$ and $\vec{n}$ is the normal vector of the plane. Both d_l and d_p are smaller and tend toward 0. Therefore, the relationship of the corresponding pairs will be more stable and accurate.

D. Motion estimation

When T_n^W is the transformation vector between the BLS point cloud and its reference point cloud, the scanner motion can be represented by 6-DOF and consists of position and attitude during a sweep, i.e.,

$$T_n^W = [t_x, t_y, t_z, \omega, \varphi, \kappa]$$

where t_x, t_y and t_z are translations along the x-, y- and z-axes, respectively. ω, φ and κ are rotation angulars around the x-, y-, z-axes, respectively. $\tilde{X}_{t+1}$ is the raw BLS point cloud at the time of sweep, $t + 1$, and X_{t+1} is the transformation result. To estimate accurate motion of the BLS system, a rigid transformation relationship between $\tilde{X}_{t+1}$ and X_{t+1} can be established:

$$X_{t+1} = R\tilde{X}_{t+1} + T_n^W(1:3) \tag{5}$$

where R is the rotation matrix ($R \in \mathbb{R}^{3\times3}$). From (3), we can derive a geometric relationship between each skeleton node in the BLS point cloud at the time of sweep, $t + 1$, and its corresponding line feature in the reference point cloud:

$$\mathbf{f}_l\left(X_{(t+1,l)}\right) = d_l \tag{6}$$

Similarly, from (4) we can derive a geometric relationship between the point feature in the current BLS point cloud and its correspondence in the reference point cloud:

$$\mathbf{f}_p\left(X_{(t+1,p)}\right) = d_p \tag{7}$$

Combining (6) and (7), a nonlinear function about T_n^W can be established:

$$\mathbf{f}(T_n^W) = \sum \mathbf{f}_l\left(X_{(t+1,l)}\right) + \sum \mathbf{f}_p\left(X_{(t+1,p)}\right) \tag{8}$$

where $\mathbf{f}(\cdot)$ represents the distance between the keypoint and its corresponding feature and each row of $\mathbf{f}$ corresponds to a feature. Finally, (8) can be solved through nonlinear iterations by minimizing the error e toward zero with the Levenberg-Marquardt (L-M) method:

$$e = arg \min_e \frac{1}{2}\sum_{i=1}^{N} \|d_i - 0\|^2 = arg \min_e \frac{1}{2}\mathbf{f}(T_n^W)^T\mathbf{f}(T_n^W) \tag{9}$$

First, we linearize (9) with the first-order approximation of a Taylor expansion:

$$\mathbf{f}(T_n^W) = \mathbf{f}(\widehat{T}_n^W + \Delta T) = \mathbf{f}(\widehat{T}_n^W) + J\Delta T \tag{10}$$

where $\widehat{T}_n^W$ is the initial motion in 6-DOF and ΔT is the correction of the initial motion. J is the Jacobian matrix of $\mathbf{f}(\cdot)$. Then, the correction ΔT can be solved by:

$$\Delta T = (J^{\mathrm{T}}J + \lambda I)^{-1}J^{\mathrm{T}}d \tag{11}$$

where λ is the damping factor, and the scanner motion can be calculated by:

$$T_n^W = \widehat{T}_n^W + \Delta T \tag{12}$$

Once T_n^W is obtained, $\tilde{X}_{t+1}$ can be converted into the reference coordinate system.

E. Global optimization

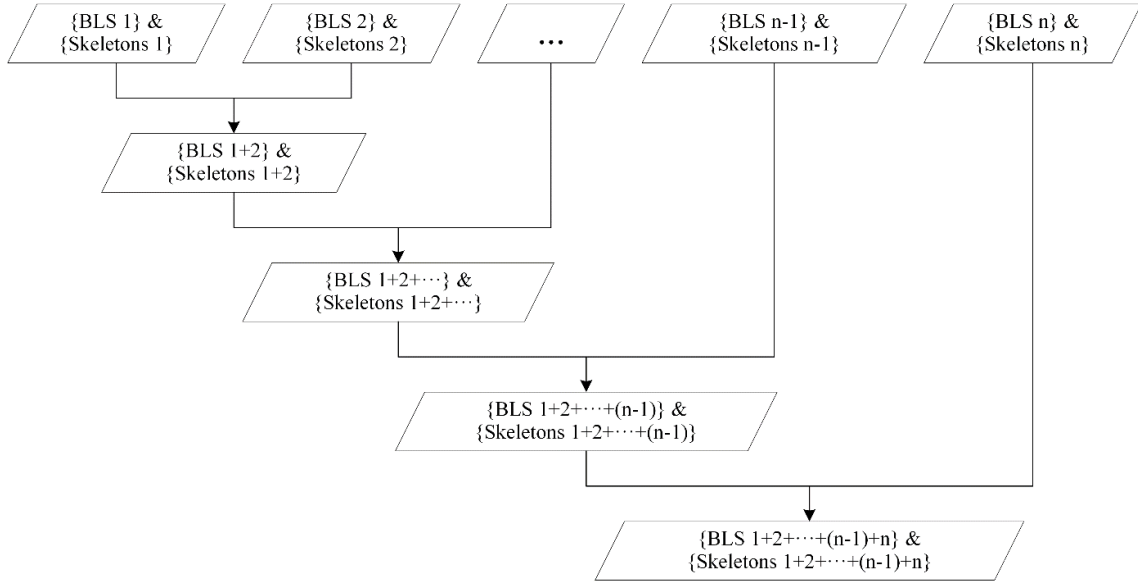To eliminate the accumulative error and transform the BLS data from different perspectives into a global coordinate system, global optimization is usually used for the SLAM process [37]. To maintain global mapping accuracy, most of the related methods need to perform numerous loop-closure detections, increasing the algorithm complexity [38]. Compared to other environments (e.g., indoor and urban), there are more occlusion effects in forest environments, but the forest plot areas are generally within the range of the LiDAR and the forest plots still have certain permeability. In other words, the objects in the previous BLS point clouds still can be observed by the subsequent BLS point clouds. Therefore, we use the previous BLS point clouds as constraints and propose an optimization framework based on two incremental maps. The two maps contain trunk skeleton points and incremental BLS point clouds. The detailed schematic is shown in Fig. 4.

Fig. 4. Schematic of global optimization. {BLS(1,2,…,n − 1, n)} and {Skeletons(1,2,…,n − 1, n)} denote BLS data and the trunk skeleton map at different times, respectively. {BLS(1 + 2 + ⋯ + n − 1 + n)} and {Skeletons(1 + 2 + ⋯ + n − 1 + n)} represent the incremental BLS point clouds and the incremental trunk skeleton map, respectively.

In the proposed optimization framework, the BLS point cloud at the time of sweep 1 and its corresponding trunk skeleton data are regarded as initial references, where the BLS point cloud is used to provide constraint for the point features and the trunk skeletons are used to provide constraint for the line features. In addition, the coordinate system of the first frame of the BLS point cloud is regarded as the global coordinate system. For the BLS point cloud at the time of sweep 2, the scanner motion is calculated according to Section II. B – II. D, and then the current point cloud is transformed into the global coordinate system; simultaneously, we rebuild the incremental BLS data and trunk skeleton points by combining the data at the time of sweep 1 and 2 and set the two incremental maps as new references for global optimization. Similarly, for each of the subsequent BLS point clouds, the motion at the time of sweep, n, adopts the motion at the time of sweep, $n - 1$, as an initial pose, and the two incremental maps provide global constraints and horizontal constraints for motion estimation, respectively; furthermore, the BLS point cloud and its corresponding trunk skeleton data will be transformed into a global coordinate system and the two global incremental maps are updated. In addition, the mean distance between the skeleton nodes and their corresponding line features are used for determining whether the current BLS point cloud is a keyframe. If the mean distance is less than the set threshold, the current BLS point cloud will be regarded as a keyframe, and then, the point cloud and its corresponding trunk skeleton data are added to the two incremental maps, respectively, of which the threshold is an empirical value and set as twice the measurement precision of the scanner.

III. EXPERIMENTAL RESULTS

A. Study area and data acquisition

The study area, located in Saihanba National Forest Park in Hebei Province in northern China, is dominated by coniferous trees. For this study, we acquired two sets of data in different plots of approximately 30 m ×30 m in size. The mean diameter at the breast height (DBH) varies between 0.25 m ~ 0.30 m in the test plots.

A single scanner BLS system is designed in this study and consists of a single scanner (Velodyne VLP-16), a data recording device (PC), and a backpack frame (a simple test system is shown in Fig. 5), where the scanner was mounted on the backpack frame. The VLP-16 supports 16 channels, collects 600,000 points/sec, and its field of view (FOV) is 360 ° in the horizontal direction and 30 ° in the vertical direction. The angular resolution is 2 ° in the vertical direction and varies between 0.1 ° ~ 0.4 ° in the horizontal direction. The maximum range is approximately 100 m and the measurement precision is around 3 cm in the 100 m range. The BLS point clouds were captured by moving around the forest plots, and the sampling frequency of the BLS was set to 10 Hz.
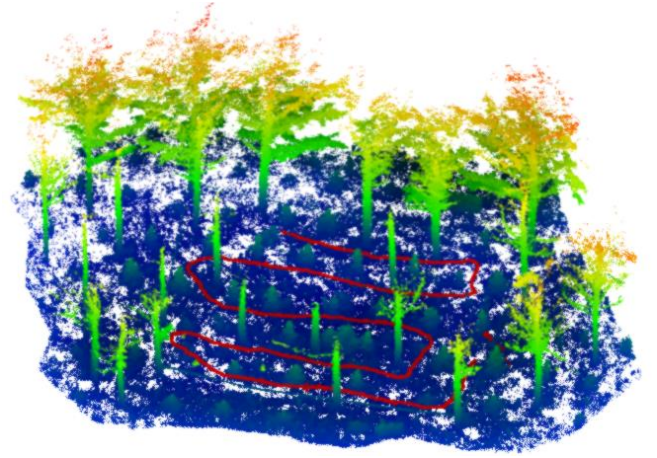

Fig. 5. The BLS system.

B. Forest plots mapping

To verify the effectiveness of the proposed method, two sets of data were collected to map forest environments using the designed BLS system. In this paper, we achieved forest plots mapping and recovered the trajectory of the BLS system (see Fig. 6).
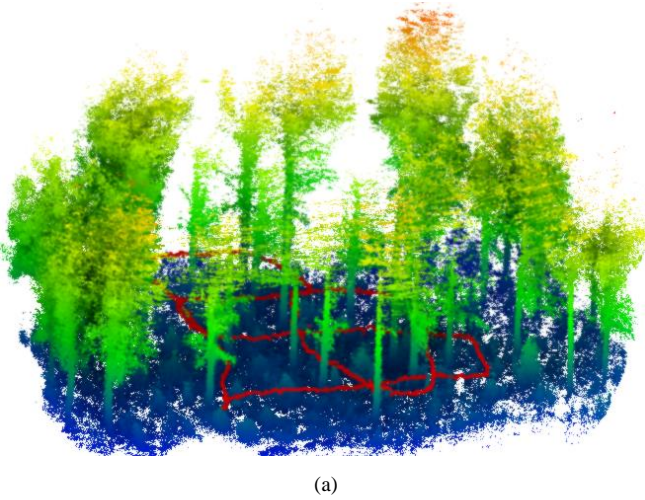
| (a) | (b) |

Fig. 6. Forest mapping results. (a) and (b) represent the mapping results of datasets 1 and 2, respectively, where red points represent the trajectories of the BLS system in the test plots.

In Fig. 6, the results show that the below-canopy structural information in the test plots are constructed by using the designed BLS system, and the trajectories are coincident with the practical movements. In the mapping results, each tree in the plots is registered with high accuracy, and the distribution of individual trees is identifiable and has no significant deviations, which suggest that the trees reconstructed by the proposed method are available in forest inventories. In addition, the trajectories of the scanner do not drift from their correct values in the two plots, e.g., the trajectory in Fig. 6 (a) is closed without a loop-closure detection process during global optimization, and the open trajectory in Fig. 6 (b) is still recovered by the proposed method, which suggests the reliability of the trajectories.

C. Mapping accuracy

Due to the impact of occlusion, the GNSS system is not reliable in below-canopy environments. In the forest, the locations of tree stems were available for evaluating planimetric accuracy. Therefore, to quantitatively evaluate the performance of the proposed method, the mapping results were compared to those from multi-scan TLS data, of which the stem position deviations, including mean absolute deviation (Mean), standard deviation (STD), and the maximum deviation (Max), were used to assess planimetric accuracy of the mapping results. In the two datasets, 17 trees and 20 trees were selected, and the centers of the tree stems at approximately 1.3 m above ground are regarded as the stem position. Then, the deviations between the stem position in the

mapping results and the corresponding positions in the multi-scan TLS data are summarized in Table I.

TABLE I
PLANIMETRIC ACCURACY

Datasets	Number of sample stems	Planimetric deviations (m)		
		Mean	STD	Max
1	17	0.0180	0.0067	0.0282
2	20	0.0157	0.0064	0.0319

From Table I, the stem position deviations indicated highly accurate results of mapping. The mean absolute deviations and the maximum deviations were at the centimeter level, of which the mean absolute deviations varied between 0.015 m and 0.020 m, and the maximum deviations were approximately 0.03 m. The standard deviations were at the millimeter level, which indicated a stable distribution. In other words, individual trees achieved similar mapping results. In addition to the stem position, the branch position can reflect the mapping accuracy in the vertical direction. Therefore, to further assess the performance, the deviations between the branch position in the mapping results and the corresponding positions in the multi-scan TLS data were calculated for evaluating the vertical accuracy. In practice, some remarkable feature points on the branches were selected. The vertical accuracies are summarized in Table II.

TABLE II
VERTICAL ACCURACY

Datasets	Number of sample points	Vertical deviations (m)		
		Mean	STD	Max
1	18	0.0182	0.0109	0.0391
2	18	0.0152	0.0088	0.0300

For forest measurements, high accuracy is generally required for the registration in the horizontal direction, which needs to meet the requirements of structural parameter (e.g., DBH) measurements. From Table II, in the test plots, the mean absolute deviations and the maximum deviations were at the centimeter level, of which the mean absolute deviations varied between 0.015 m and 0.020 m, and the maximum deviations were greater than 0.03 m. The standard deviations were approximately 0.01 m, which indicated a certain stability of the results. In general, the requirement of the vertical accuracy is lower than the horizontal accuracy for forest measurements (e.g., tree height), so the accuracies indicated effectiveness of the mapping results. Overall, the proposed global optimization framework based on two incremental maps can achieve BLS-based forest mapping, of which the two incremental maps provide effective global consistency constraints for each BLS point cloud. In particular, the trunk skeletons map maintained the accuracies of positioning and mapping in the horizontal direction, and the incremental BLS point clouds provided global consistency constraint for forest mapping in the vertical direction.

IV. DISCUSSION

A. Comparison of motion estimation

In this paper, line and point features were used to solve the planimetric and vertical errors of registration in forest environments, respectively. To assess the effectiveness of the features in motion estimation, we analyzed two frame BLS point clouds registration results according to stems and ground position deviations and compared the proposed method with two methods: the ICP and LOAM methods.

To evaluate the planimetric accuracy, 12 trees and 8 trees were selected from the two datasets, respectively, to calculate the stem position deviations. Due to the sparsity of the stem point cloud, we projected stem points to a plane and estimated the centers of the circles by the least square method. Then, the centers were regarded as stem positions, and the distances between the stem positions in the registered point cloud and their corresponding stem positions in reference were calculated. The stem position deviations were summarized in Table III.

TABLE III
PLANIMETRIC DEVIATIONS

Datasets	Methods	Number of stems	Planimetric deviations (m)		
			Mean	STD	Max
1	LOAM	12	0.0908	0.0371	0.1430
	ICP	12	0.0359	0.0167	0.0593
	Proposed method	12	0.0192	0.0097	0.0408
2	LOAM	8	0.0465	0.0296	0.1019
	ICP	8	0.0384	0.0144	0.0639
	Proposed method	8	0.0251	0.0076	0.0339

In Table III, the results from the LOAM and ICP methods show greater deviations than those of the proposed method, especially the LOAM method. The mean absolute deviations calculated by the LOAM methods are 0.0908 m and 0.0465 m for the two datasets, and the standard deviations are approximately 0.03 m and the maximum deviations are greater than 0.1 m, which show large deviations. The mean absolute deviations of the ICP method varies between 0.035 m and 0.04 m, and the standard deviations and maximum deviations are approximately 0.015 m and 0.06 m, respectively. In contrast, the proposed method performs well, of which the mean absolute deviations are 0.0192 m and 0.0251 m in the two datasets, the standard deviations are at the millimeter level, and the maximum deviation is 0.0408 m. The LOAM method estimates motion, combining the line and plane features, and requires initial motion information, which is generally provided by an IMU system. However, there is no initial motion information for the LOAM method in this paper, and the stable geometrical features are difficult to extract directly from the forest environments. Consequently, because there is no strong constraint in the horizontal direction, the inaccurate corresponding pairs in the adjacent BLS point clouds cause the LOAM method to fall into a local minima and caused large planimetric errors. In addition, the point-to-point ICP method was adopted to estimate the motion of the BLS system, which considers all points in registration and generally requires high overlap of point clouds. Although the BLS point clouds were acquired in adjacent locations, there are certain errors in the matching of the two adjacent BLS point clouds because of the sparsity of the BLS data. In contrast, the proposed line features (the trunk skeleton lines) are stable and can provide a strong constraint for scan matching in the horizontal direction, so the proposed method obtained small stem position deviations.

In addition to the planimetric error, we also analyzed the vertical error based on the branch position deviations. In the two datasets, some remarkable feature points on the ground were selected to verify the proposed method. We then calculated the distance between the sample points in the registered point cloud and their correspondences in reference. The vertical deviations are summarized in Table IV.

TABLE IV
VERTICAL DEVIATIONS

Datasets	Methods	Number of points	Vertical deviations (m)		
			Mean	STD	Max
1	LOAM	22	0.0067	0.0032	0.0158
	ICP	21	0.0612	0.0439	0.1439
	Proposed method	24	0.0081	0.0051	0.0231
2	LOAM	19	0.0091	0.0059	0.0230
	ICP	20	0.0772	0.0308	0.1332
	Proposed method	20	0.0072	0.0052	0.0248

As seen in Table IV, the vertical deviations from the LOAM method and the proposed method show approximate performance, in which the mean deviations and the standard deviations are at the millimeter level in the two datasets and indicate highly accurate scan matching. In contrast, the ICP method shows large vertical deviations, of which the mean absolute deviations are greater than 0.06 m and the maximum deviations are greater than 0.1 m in the two datasets. The LOAM method and the proposed method extracted some uniform distributed features from the object surface, including some points of the ground and branches. Due to strong constraints from the ground and branches, the LOAM method and the proposed method perform well in the vertical direction. In contrast, due to the specific attributes of the scanner, the BLS point cloud is sparse in the vertical direction, and there is low overlap between the point clouds acquired from different perspectives. Consequently, uneven ground and sparse branch points are difficult to provide effective constraints and accurate corresponding pairs for scan matching.

Combining the results in Table III and Table IV, the major difference between the LOAM method and the proposed method is shown in the planimetric deviations. The proposed method estimates the motion of the BLS system without initial motion information, of which the proposed trunk skeletons features provide accurate corresponding pairs and effectively solve the problem of inaccurate registration in the horizontal direction and then ensure the planimetric accuracy of forest mapping. Meanwhile, compared to the ICP method, the point-to-plane correspondence of the proposed method can provide effective constraint and maintain the vertical accuracy. Overall, the proposed method can be suggested as a reliable mapping method in forest environments.

B. Data performance

The BLS system integrated a single scanner which was placed horizontally, such that abundant below-canopy data was acquired, but the canopy and above-canopy information were limited by the field of view of the scanner. Therefore, to analyze applications of the mapping results in forest measurements, we selected an important forest parameter, DBH below the canopy, to assess the effectiveness of the mapping results. We calculated the DBH values in the test plots and compared with those from the multi-scan TLS data. The DBH of individual trees is determined by extracting a cross section of the point cloud that falls between 1.2 m and 1.4 m above the ground level. First, we filtered the ground and non-ground points [39] and extracted points that represented the tree stem hull at the breast height from the non-ground points and then used the least square method to fit a circle. 16 trees and 14 trees were selected for the measurement of DBH values in the two test plots, respectively. The accuracy of the DBH values is assessed by treating the reference as a variable that is dependent upon the fitted measurement and running a simple linear regression analysis to determine the coefficient of determination (R^2) for the two datasets (Fig. 7).
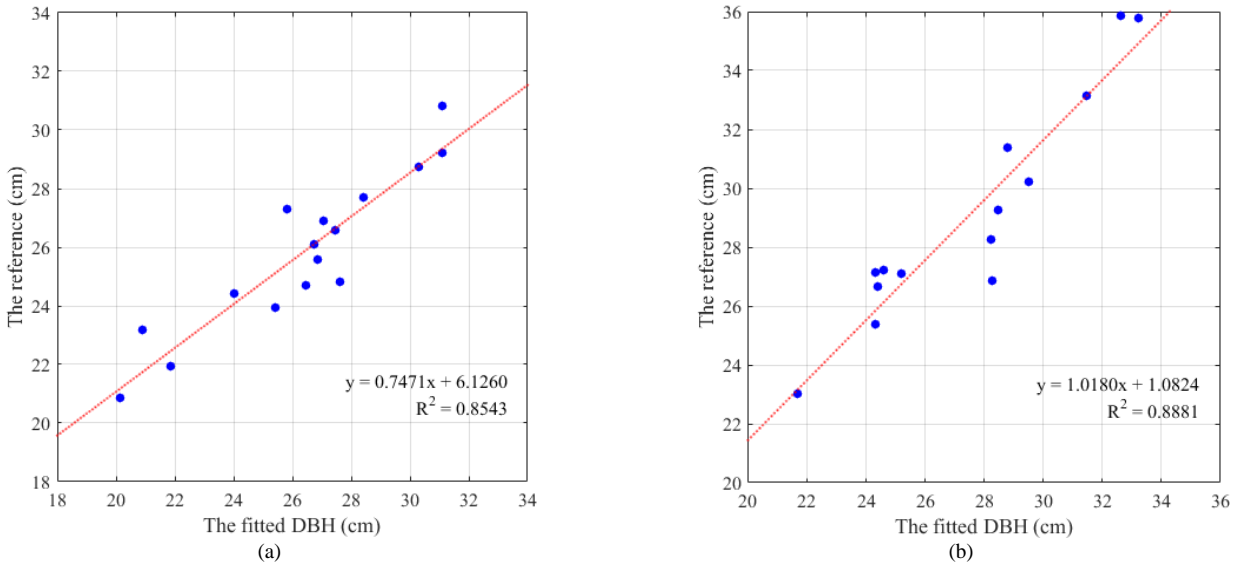

Fig. 7. Scatter plots of the DBH values. The y-axis represents the reference of DBH values from the multi-scan TLS point cloud and the x-axis represents the fitted DBH from the results of the proposed method. (a) and (b) represent dataset 1 and 2, respectively.

In Fig. 7, the results of the linear regression analysis revealed that the coefficient of determination between the fitted DBH, measured from the data via the proposed method and the fitted DBH from the multi-scan TLS data, are greater than 0.85 in the test plots, which indicated a significant correlation between the DBH measured from the proposed method and the multi-scan TLS data. In dataset 1, the root mean square error (RMSE) is 1.38 cm and the mean absolute error (MAE) is 1.15 cm, of which the total error is approximately 95.5%. In dataset 2, the RMSE between the fitted DBH values and the field measured DBH values is 1.99 cm and the MAE is 1.78 cm, and the total error is approximately 93.9%. Overall, in the test plots, the total errors are more than 90.0%, which indicated reliable stem mapping results. Therefore, the results suggested the effectiveness of the proposed line features and optimization framework for maintaining the planimetric accuracy of the mapping results.

V. CONCLUSIONS

LiDAR-based mapping has been one of the most important developments for forest measurements. To achieve fast forest mapping, this paper designed a single scanner BLS system and proposed a new mapping method. The system is simple and specific to forest environments. Subsequently, practical experiments were implemented to evaluate the effectiveness and reliability of the designed BLS system and the proposed method. In practice, the BLS system took only a few minutes to scan a forest plot, and its efficiency is significantly higher than that of the TLS method. To achieve accurate scan matching, the line features derived from the tree trunk skeletons was proposed and used to estimate the motion of the BLS system, and the line feature effectively solved the inaccurate registration problem caused by insufficient point overlap and inaccurate matching pairs in the horizontal direction. Compared to the existing methods, the matching results from the proposed method were more accurate. In addition, the global optimization framework based on the incremental BLS point clouds and the tree trunk skeleton points provided effective global consistency constraints for the BLS-based SLAM in the forest environments and ensured positioning accuracies without a GNSS-IMU system or loop-closure detection process, of which the incremental trunk skeleton points maintained accurate registration of all individual trees, especially tree stems.

Fast acquisition of abundant structural information is always expected in forest measurements. Although the proposed method achieved fast data acquisition in forest plots, the data acquired by a single scanner were limited below the canopy. In the future, therefore, to acquire more complete information, two scanners will be considered, of which one is placed horizontally for the SLAM technique and below-canopy information acquisition and the other vertically for canopy information acquisition.

REFERENCES

[1] X. Liang et al., "Terrestrial laser scanning in forest inventories," *ISPRS J. Photogramm. Remote Sens.*, vol. 115, pp. 63-77, May 2016.

[2] J. Hyyppä, "Feasibility for estimation of single tree characteristics using laser scanner," *International Geoscience and Remote Sensing Symposium*, vol. 3, pp. 981-983, 2000.

[3] G. E. Murphy, M. A. Acuna, and T. Dumbrell, "Tree value and log product yield determination in radiate pine (Pinus radiate) plantations in Australia: comparisons of terrestrial laser scanning with a forest inventory system and manual measurements," *Can. J. For. Res.*, vol. 40, no. 11, pp. 2223-2233, Oct. 2010.

[4] L. Luo et al., "Airborne and spaceborne remote sensing for archaeological and cultural heritage applications: a review of the century (1907-2017)," *Remote Sens. Environ.*, pp. 232, 2019.

[5] H. Latifi et al., "Forest inventories by LiDAR data: A comparison of single tree segmentation and metric-based methods for inventories of a heterogeneous temperate forest," *International Journal of Applied Earth Observations and Geoinformation*, vol. 42, pp. 162–174, Oct. 2015.

[6] P. Wilkers et al., "Data acquisition considerations for terrestrial laser scanning of forest plots," *Remote Sens. Environ.*, vol. 196, pp. 140-153, Jul. 2017.

[7] G. J. Newnham et al., "Terrestrial laser scanning for plot-scale forest measurement," *Curr. Forestry Rep.*, vol. 1, no. 4, pp. 239-251, Dec. 2015.

[8] S. Bauwens, H. Bartholomeus, K. Calders, and P. Lejeune, "Forest inventory with terrestrial LiDAR: a comparison of static and hand-held mobile laser scanning," *Forests*, vol. 7, no. 6, pp. 127, Jun. 2016.

[9] J. L. Lovell, V. Haverd, D. L. B. Jupp, and G. J. Newnham, "The canopy semi-analytic p gap and radiative transfer (CanSPART) model: validation using ground based LiDAR," *Agric. For. Meteorol.*, vol. 158-159, pp. 1-12, Jun. 2012.

[10] W. Zhang et al., "Efficient registration of terrestrial LiDAR scans using a coarse-to-fine strategy for forestry applications," *Agric. For. Meteorol.*, vol. 225, pp. 8-23, Sep. 2016.

[11] A. Kukko, H. Kaartinen, J. Hyyppä, and Y. Chen, "Multiplatform mobile laser scanning: usability and performance," *Sensors*, vol. 12, no. 9, pp. 11712-11733, Dec. 2012.

[12] X. Liang et al., "The use of a mobile laser scanning system for mapping large forest plots," *IEEE Geosci. Remote Sens. Lett.*, vol. 11, no. 9, pp. 1504-1508, Jan. 2014.

[13] M. Miettinen, M. Ohman, A. Visala, and P. Forsman, "Simultaneous localization and mapping for forest harvesters," *In Proceedings of the IEEE International Conference on Robotics and Automation (ICRA)*, pp. 517-522, Apr. 2007.

[14] M. Holopainen et al., "Tree mapping using airborne, terrestrial and mobile laser scanning – a case study in a heterogeneous urban forest," *Urban For. Urban Green.*, vol. 12, no. 14, pp. 546-553, Jul. 2013.

[15] L. Chang et al., "GNSS/INS/LiDAR-SLAM integrated navigation system based on graph optimization," *Remote Sens.*, vol. 11, no. 9, pp. 1009, Apr. 2019.

[16] J. Tang et al., "SLAM-aided stem mapping for forest inventory with small-footprint mobile LiDAR," *Forests*, vol. 6, no. 12, pp. 4588-4606, Dec. 2015.

[17] A. Kukko et al., "Graph SLAM correction for single scanner MLS forest data under boreal forest canopy," *ISPRS J. Photogramm. Remote Sens.*, vol. 132, pp. 199-209, Oct. 2017.

[18] M. W. M. G. Dissanayake et al., "A solution to the simultaneous localization and map building (SLAM) problem," *IEEE Transactions on Robotics and Automation*, vol. 17, no. 3, pp. 229-241, Jun. 2001.

[19] M. Pierzchała, P. Giguère, and R. Astrup, "Mapping forests using an unmanned ground vehicle with 3D LiDAR and graph-SLAM," *Comput. Electron. Agr.*, vol. 145, pp. 217-225, Feb. 2018.

[20] A. J. Davison, I. D. Reid, N. Molton, and O. Stasse, "MonoSLAM: real-time single camera slam," *IEEE Transactions on Pattern Analysis and Machine Intelligence*, vol. 29, no. 6, pp. 1052-1067, Jun. 2007.

[21] J. Engel, T. Schöps, and D. Cremers, "LSD-SLAM: large-scale direct monocular slam," *European Conference on Computer Vision*, pp. 834-849, 2014.

[22] C. Forster, M. Pizzoli, and D. Scaramuzza, "SVO: fast semi-direct monocular visual odometry," *IEEE International Conference on Robotics and Automation (ICRA)*, pp. 15-22, 2014.

[23] R. Mur-Artal, J. Montiel, and J. D. Tardós, "ORB-SLAM: a versatile and accurate monocular slam system," *IEEE Trans. Robot.*, vol. 31, no. 5, pp. 1147-1163, Aug. 2015.

[24] J. Zhang, and S. Singh, "LOAM: lidar odometry and mapping in real-time," *Robotics: Science and Systems Conference*, 2014.

[25] W. Hess, D. Kohler, H. Rapp, and D. Andor, "Real-time loop closure in 2d lidar slam," *IEEE International Conference on Robotics and Automation (ICRA)*, 2016.

[26] C. Qian et al., "An integrated GNSS/INS/LiDAR-SLAM positioning method for highly accurate forest stem mapping," *Remote Sens.*, vol. 9, no. 1, pp. 3, Dec. 2017.

[27] X. Yang et al., "Three-dimensional forest reconstruction and structural parameter retrievals using a terrestrial full-waveform lidar instrument (Echidna R)," *Remote Sens. Environ.*, vol. 135, pp. 36-51, Aug, 2013.

[28] T. Aschoff, M. Thies, and H.Spiecker, "Describing forest stands using terrestrial laser-scanning," *Int. Archives Photogramm., Remote Sens. Spatial Inf. Sci.*, vol. 35, pp. 237-241, 2004.

[29] G. Zheng, and L. M. Moskal, "Computational-geometry-based retrieval of effective leaf area index using terrestrial laser scanning," *IEEE Trans. Geosci. Remote Sens.*, vol. 50, no. 10, pp. 3958-3969, Jun. 2012.

[30] D. Kelbe et al., "Marker-free registration of forest terrestrial laser scanner data pairs with embedded confidence metrics," *IEEE Trans. Geosci. Remote Sens.*, vol. 54, pp. 4314-4330, Apr. 2016.

[31] P. Polewski, W. Yao, L. Cao, and S. Gao, "Marker-free coregistration of UAV and backpack LiDAR point clouds in forested areas," *ISPRS J. Photogramm. Remote Sens.*, vol. 147, pp. 307-318, Jan. 2019.

[32] D. Van der Zander et al., "Influence of measurement set-up of ground-based LiDAR for derivation of tree structure," *Agricultural Forest Meteorol.*, vol. 141, no. 2, pp. 147-160, Dec. 2006.

[33] P. J. Besl, N. D. Mckay. A method for registration of 3-D shapes. *IEEE T. Pattern Anal.*, vol. 14, no. 2, pp. 239-256, Feb. 1992.

[34] R. Cifuentes et al., "Effects of voxel size and sampling setup on the estimation of forest canopy gap fraction from terrestrial laser scanning data," *Agricultural Forest Meteorol.*, vol. 194, no. 15, pp. 230-240, Aug. 2014.

[35] W. Zhang et al., "A novel approach for the detection of standing tree stems from plot-level terrestrial laser scanning data," *Remote Sens.*, vol. 11, no. 2, pp. 211, Jan. 2019.

[36] P. W. Theiler, J. D. Wegner, and K. Schindler, "Keypoint-based 4-points congruent sets – automated marker-less registration of laser scans," *ISPRS J. Photogramm. Remote Sens.*, vol. 96, pp. 149-163, Oct. 2014.

[37] J. Shao et al., "Automated markerless registration of point clouds from TLS and structured light scanner for heritage documentation," *J. Cult. Herit.*, vol. 35, pp. 16-24, 2019.

[38] M. Labbé, and F. Michaud, "Online global loop closure detection for large-scale multi-session graph-based SLAM," *In Proc. of the IEEE/RSJ International Conference on Intelligent Robots and Systems*, 2014.

[39] W. Zhang et al., "An easy-to-use airborne LiDAR data filtering method based on cloth simulation," *Remote Sens.*, vol. 8, no. 6, pp. 501, Jun. 2016.